Optical Modulation of Azobenzene-Modified Peptide for Gold Surface Binding

Joseph M. Slocik,[a] Zhifeng Kuang,[a] Marc R. Knecht,[b] and Rajesh R. Naik*[c]

The ability to precisely and remotely modulate reversible binding interactions between biomolecules and abiotic surfaces is appealing for many applications. To achieve this level of control, an azobenzene-based optical switch is added to nanoparticle-binding peptides in order to switch peptide conformation and attenuate binding affinity to gold surfaces via binding and dissociation of peptides.

1. Introduction

The ability to effectively manipulate the binding interactions between biomolecules and nanomaterial surfaces is an important goal to achieving reconfigurable materials with enhanced properties and nanostructures for sensing, catalysis, and biomedical applications. However, this is dependent on understanding the mutually complex effects of peptide/protein sequence and secondary structure on binding and designing biomolecules that can adopt multiple different conformational states. A wealth of biomolecules with unique sequences has provided insight into binding interactions with many inorganic surfaces.[1] These include nanoparticle-binding peptides isolated from phage displayed peptide libraries, naturally occurring peptides/proteins associated with biogenic inorganic materials, short oligonucleotides, and small metal-binding proteins.[2–4] In total, biomolecule-nanoparticle interactions have resulted in peptides with high binding affinities and materials with emergent functional properties, increased stabilities, complex assembled nanostructures, and increased catalytic activities.[5,6] However, refining these complex relationships will lead to materials with improved properties and tunable interactions.

Importantly, the binding of biomolecules to inorganic surfaces is greatly influenced by changes to its structure and conformation. Peptides are capable of adopting multiple conformations by means of unfolding and restructuring under certain conditions. Current biochemical approaches to induce peptide structural changes have involved substituting amino acids at key hot-spot positions in order to insert turns or break long structured sections, employing molecular conformation constraints (loops, cyclic structures), and/or utilizing different environmental conditions and structure-directing agents (high salt concentrations, surfactants, chaotropes, organic solvents, enzymes, and high temperatures).[8–14] All of these methods affect peptide structure and nanomaterial binding, but require chemical modification, denaturing conditions, and addition or removal of high concentrations of structure-enhancing solvents (i.e. trifluoroethanol, 6 M guanidinum) to reverse structure change. Also, these conditions potentially alter the nanomaterial structure/morphology, impart surface defects, and/or contaminate the nanomaterial surface.[12,14] Collateral damage to the material ultimately leads to changes in physiochemical properties.[7,8]

Biological systems control protein structure as a means to promote various cell signaling and binding processes. Reversible biomolecular binding interactions are accomplished by employing molecules with weak to moderate binding affinities, by changing protein structure/shape/geometry to modulate interactions in response to a stimuli or formation of a product, and/or by regulating oxidation states of active binding sites.[15,16] Biomimetically, similar control over binding and peptide structure has recently been achieved with small peptides by incorporating an azobenzene photoswitch to control gene regulation, enzyme inhibition, and inorganic surface interfaces.[9–11,17] In the latter example, attachment of azobenzene at the N- or C-terminus of a peptide led to rapid reorganization of the peptide–nanoparticle interface, but did not have a direct influence on binding interactions.[17] In this study, we have exploited the photoisomerization properties of azobenzene to create a photoresponsive nanomaterial-binding peptide that is capable of modulating interactions from weak to strong binding to a gold surface using light. Our intent was to examine whether an azobenzene cross-linker can be used to control binding and dissociation with an inorganic surface by light as a result of changing the peptide conformation. The azobenzene optical trigger

[a] Dr. J. M. Slocik, Dr. Z. Kuang
Soft Matter Materials Branch
Materials and Manufacturing Directorate
Air Force Research Laboratory
Dayton, OH 45433 (USA)

[b] Prof. M. R. Knecht
Department of Chemistry
Miami University
Miami, FL 33146 (USA)

[c] Dr. R. R. Naik
711th Human Performance Wing
Air Force Research Laboratory,
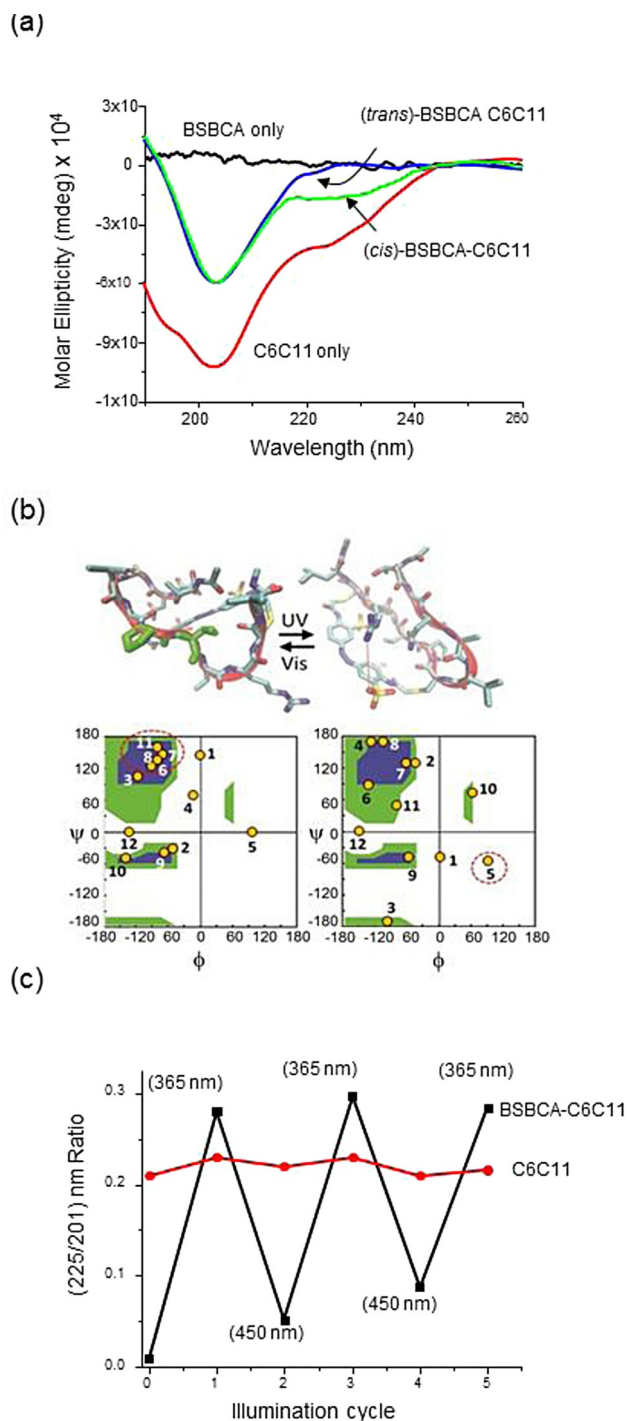Dayton OH 45433 (USA)
E-mail: rajesh.naik@us.af.mil

Supporting Information for this article can be found under:
http://dx.doi.org/10.1002/cphc.201600670.

incorporated into a strong peptide binder promotes an intra-peptide conformational change and regulates gold surface interactions. This approach provides a means to bind/release peptides from surfaces on demand, understand the role of peptide structure on surface binding, and to control nanoparticle sizes during biomimetic synthesis of nanomaterials.

2. Results and Discussion

To obtain a photoswitchable nanoparticle-binding peptide, we modified a palladium-binding peptide (C6C11), with a water-soluble sulfonated azobenzene-based thiol-reactive 3,3′-bis(sulfonato)-4,4′-bis(chloroacetamido)-azobenzene (BSBCA) cross-linker to form an intrapeptide optical switch.[6, 12] BSBCA cross-linkers photoisomerize between *trans* and *cis* states upon irradiation with 365 nm UV light (10 mW cm^{-2}) or visible light at 450 nm (9 mW cm^{-2}). BSBCA exhibits moderate thermal relaxation rates of several minutes, and can be incorporated into a peptide sequence via peptide side-chain groups rather than the backbone to maximize structural changes.[13] From previous studies, it is known that cysteine residues located at the 6 and 11 amino acid positions within the C6C11 peptide (TSNAV**C**PTLR**C**L) are exposed to the bulk solvent, reside on the same peptide face, and exhibit high binding affinity to palladium and gold surfaces.[6, 14] As a result, these cysteine residues provide favorable spacing for conjugation of the BSBCA cross-linker. Conjugation of BSBCA cross-linker to the C6C11 peptide was performed by following a previously reported procedure.[12] The BSBCA modified peptide was purified by reversed phase HPLC on a C$_{18}$ column and characterized by UV/Vis spectrosopy (Figure S1). After conjugation and purification, we observed an increase in the *cis→trans* isomerization half-life ($t_{1/2}$) of the BSBCA modified peptide ($t_{1/2} = 24.4 \pm 0.9$ min) as compared to free BSBCA ($t_{1/2} = 11.0 \pm 1.1$ min) by monitoring the absorbance at 365 nm (Figure S1). The longer half-life for BSBCA-C6C11 is due to a constrained structure and is consistent with the half-life of other BSBCA cross-linked peptides.[12, 21] Analysis of the *cis* isomer populations produced by UV exposure showed a maximum population of 80% free *cis*-BSBCA (no peptide) and ≈53% (*cis*)-BSBCA-C6C11 peptide in solution based on absorbance at 365 nm. The decreased *cis* fraction is likely due to creation of forbidden electronic transition states of BSBCA and/or are sterically blocked by the formation of multiple different peptide–BSBCA configurations which prevents isomerization previously observed in other studies.
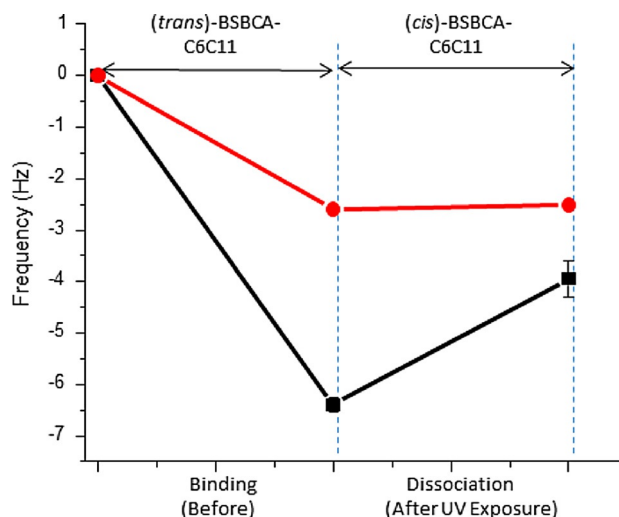
We first examined the structural effect of attaching the BSBCA cross-linker to the C6C11 peptide using CD spectroscopy (CD). Addition of BSBCA resulted in a loss of helicity and disappearance of the CD peak at 225 nm (Figure 1a) due to peptide unfolding in order to accommodate the cross-linked azobenzene. However, exposure of BSBCA-C6C11 peptide with UV light (*trans→cis*) produced an increase in negative ellipticity in the 220–240 nm region and the appearance of a peak at 225 nm (Figure 1a), while the CD spectrum of the unmodified parent C6C11 peptide remained unchanged upon exposure to UV (Figure S6). Comparison to known CD spectra of character-

Figure 1. a) Circular dichroism spectra of unmodified C6C11 peptide, *trans*-BSBCA-C6C11, and *cis*-BSBCA-C6C11 in water at concentrations of 19 μM. BSBCA-C6C11 was irradiated at 365 nm using a CD spectrometer for 20 minutes and a CD spectrum was immediately collected in the dark to reduce relaxation back to *trans*. Molar ellipticity is in deg cm^2 dmole^{-1}. b) Top: Computationally predicted conformation of *trans*-BSBCA-C6C11 peptide containing PPII left helix content marked in green and of *cis*-BSBCA-C6C11 showing unordered coil. Bottom: Corresponding Ramachandran plots using 1000 snapshots of *trans*-BSBCA-C6C11, where the PPII region is circled in red dashes and 1000 snapshots of *cis*-BSBCA-C6C11 where Val-5 is circled in red. Residues in Ramachandran plot are labelled by residue number T^{1}S^{2}N^{3}A^{4}V^{5}C^{6}P^{7}T^{8}L^{9}R^{10}C^{11}L^{12}. c) Photoswitching cycles of the BSBCA-C6C11 peptide and unmodified C6C11 peptide as control, showing reversibility of peptide structures plotted as ratio of ellipticity at 225 nm and 201 nm from respective CD spectra upon irradiation at 365 nm or 450 nm.

istic protein secondary structures, the *trans*-BSBCA-C6C11 peptide possesses a CD spectrum indicative of a polyproline type II (PPII) helical conformation with negative and positive bands at 201 nm and 225 nm, respectively, whereas the CD spectrum of the *cis*-BSBCA-C6C11 peptide contains features representative of unordered random coils.[19, 20] Deconvolution of CD spectra further showed *trans*-BSBCA-C6C11 to contain a higher fraction of β-sheets, but a lower fraction of turns relative to *cis*-BSBCA-C6C11 (Figure S2). To further probe the conformational change, we also used computational modelling to examine the conformations of both *trans*-BSBCA-C6C11 and *cis*-BSBCA-C6C11 using replica exchange molecular dynamics simulations using 64 replicas with temperature ranging from 280 to 680 K in explicit water (Figure 1 b). In the *trans*-BSBCA-C6C11 structure, a PPII left turn occurs at residues Pro-7 and Thr-8; while the *cis*-BSBCA-C6C11 structure shows a turn at Val-5 and the formation of an important salt bridge between Arg10 and the negatively charged sulfonate group in the linker (Figure 1 b). The enhanced stability imparted by the salt bridge in (*cis*)-BSBCA-C6C11 is also reflected in the longer isomerization half-life determined experimentally. Therefore, both experimental observation and computational prediction consistently show notable peptide structure changes induced by the isomerization of the linker. In previous peptide-azobenzene systems, the structure change of the peptide was found to be highly dependent upon the cross-linker attachment sites within the peptide sequence as previously shown,[13, 21] while in others utilizing only a monofunctionalized azobenzene terminal moiety, there was minimal structure change. The conformation of BSBCA-C6C11 exhibited reversibility upon cycling between light at 365 nm and 450 nm over multiple cycles, wherein its stable *trans* form loses ellipticity at 225 nm (Figure 1 c; Figure S3).

The structure and conformation of biomolecules significantly impacts how peptides interact with nanomaterial surfaces.[22] Given the switchable peptide conformations of the BSBCA-C6C11 peptide, we used a quartz crystal microbalance with dissipation (QCM-D) to measure both binding and light induced dissociation from a gold and palladium surface in situ as a function of illumination via a UV-IR transparent sapphire window integrated QCM flow cell module. For binding, we first saturated a gold or palladium surface with *trans*-BSBCA-C6C11 peptide and obtained a frequency decrease of ≈ 7 Hz or ≈ 3.5 Hz (Figure 2). After binding to gold or palladium, the *trans*-BSBCA-C6C11 peptide was converted to *cis*-BSBCA-C6C11 by illumination with a 365 nm light source (Spitfire UV 365 nm LED flashlight, 25 mW cm^{-2} actual light intensity) through the sapphire window port. During illumination, we collected the peptide released from the gold surface in a centrifuge tube in order to separate *cis*- and *trans*-peptide populations (53% *cis*/47% *trans*). For gold, *trans*-BSBCA-C6C11→*cis*-BSBCA-C6C11 isomerization resulted in a slow frequency increase indicating a loss of mass of *cis*-BSBCA-C6C11 from the surface. After the UV source was turned off and equilibration was reached, we observed an approximate 40 wt% loss of peptide from the gold surface (Figure 2). The loss of peptide from the gold surface is due to a change in the peptide conformation and a weaker binding affinity of the peptide in the *cis*-state (Table 1). The partial loss

Figure 2. Frequency change of the *trans* and *cis* conformation of BSBCA-C6C11 on a gold- (black squares) or palladium-coated (red circles) surface obtained using QCM. QCM surfaces were irradiated using a Spitfire 3W 365 nm LED flashlight held approximately 1 cm above the sapphire window. The flow rate was set to 0.17 mL min^{-1} for peptide binding and changed to 0.35 mL min^{-1} during peptide dissociation from gold or palladium surfaces.

Table 1. Binding constants of *trans* and *cis*-conformations of peptides to a gold surface obtained using QCM.

Peptide	$K_{eq} \times 10^5$ [M^{-1}]
trans-BSBCA-C6C11	12.0 ± 1.9
cis-BSBCA-C6C11	2.5 ± 0.18
trans-BSBCA-C6C11-R	4.6 ± 0.31
cis-BSBCA-C6C11-R	0.4 ± 0.04

of peptide (40 wt%) is consistent with a maximum population of $\approx 53\%$ *cis*-BSBCA-C6C11 generated during UV irradiation in solution. Notably, the peptide fraction collected from gold during UV illumination is enriched to 99.5% of *cis*-BSBCA-C6C11 peptide according to UV/Vis analysis (Figure S4). In contrast, the *trans*-BSBCA-C6C11 isomer fraction remained strongly bound to the gold surface enabling the separation of *cis* peptides. To date, there is no analytical technique or chromatographic method (i.e. chiral chromatography) to completely and efficiently separate mixed populations of short-lived *cis*/*trans* isomers. Consequently, when we used the enriched population of *cis* peptides with gold (converted to *trans* for gold binding), we observed an increase in the loss of peptide (82.8%) from the surface after UV exposure (Figure S4). This approach enabled maximal enrichment and separation of *cis* peptides released off gold from non-isomerizable *trans* peptides remaining bound to gold.

Moreover, we could repopulate the open binding sites left on the gold surface by flowing in fresh *trans*-BSBCA-C6C11 peptide across gold. To further confirm these differences on gold, we determined the binding affinity of the BSBCA-C6C11 peptide in the *trans* and *cis* forms. By QCM, the affinity of UV exposed *cis*-BSBCA-C6C11 decreased as reflected by a K_{eq} of 2.5×10^5 M^{-1} and a 4-fold increase in the dissociation constant
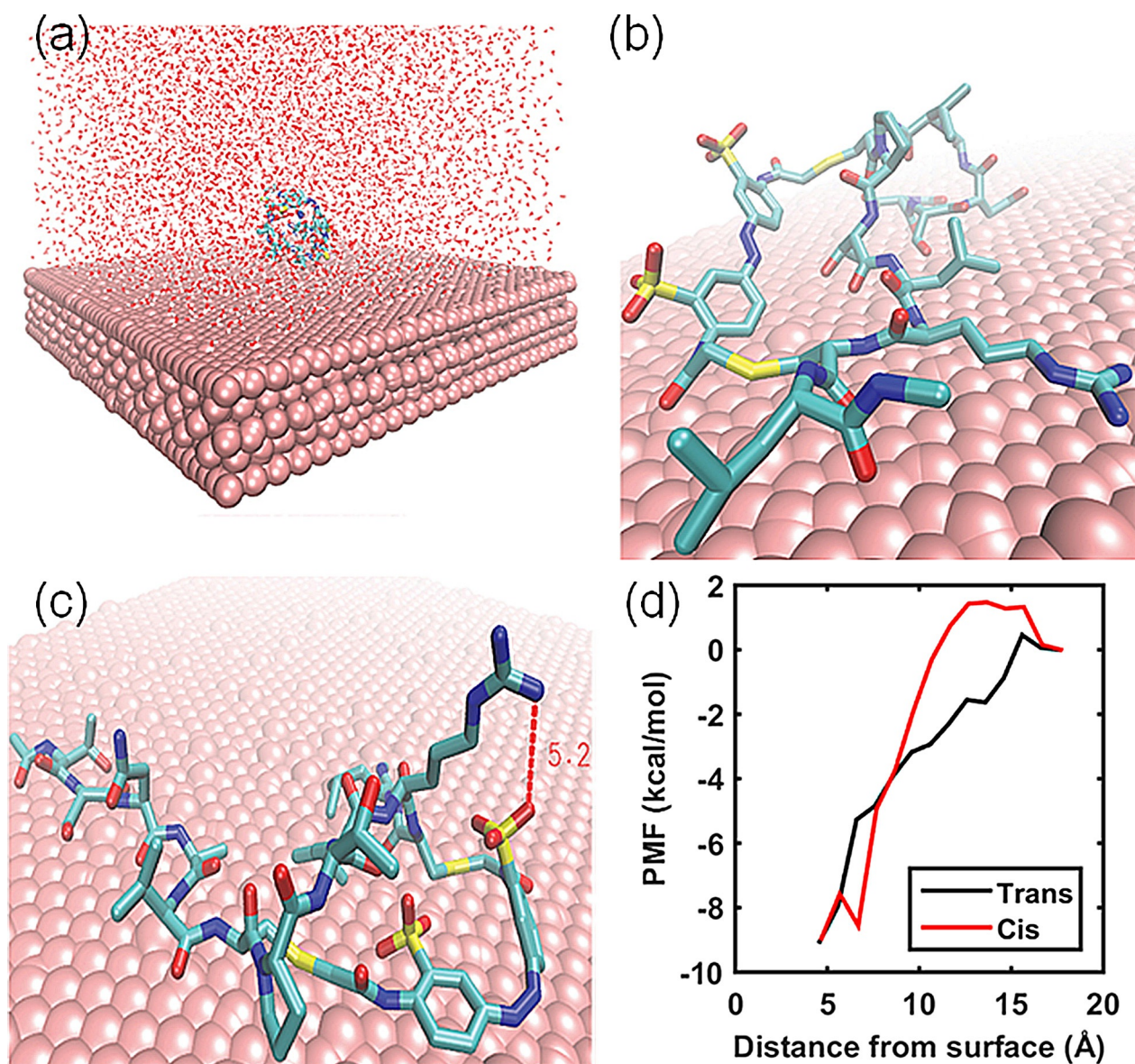
(k_d) of $5.6 \times 10^{-3} \, s^{-1}$ due to a mixed population of *cis* and *trans* forms (Table 1). Invariably, this is most likely due to a newly adopted peptide structure resulting in loss of binding/contact sites with gold surface. The effect of peptide conformation on gold binding was previously demonstrated using a linear and cyclic form of a different gold-binding peptide.[23]

As a control, we ruled out binding of the BSBCA cross-linker only (no peptide) to gold by measuring an unchanged *cis*→*trans* half-life of 11.3 ± 1.5 min vs. free BSBCA. Alternatively, when the gold surface was substituted for a palladium surface, the *cis*-BSBCA-C6C11 peptide could not be displaced from Pd after prolonged exposure to UV (Figure 2). This is due to strong interactions with the sulfonic acid groups of the BSBCA cross-linker (no peptide).[24] Binding preference of the BSBCA group (no peptide) to Pd was also confirmed by a long and irregular half-life, XPS analysis, and by the aqueous stabilization of palladium nanoparticles (Figure S5). Irreversible binding to Pd could easily be resolved by removal of the sulfonic acid groups from BSBCA and/or use of a different photo-isomerizable cross-linker. Nevertheless, Pd could potentially be used as a scavenger for *cis*-BSBCA-C6C11 peptide in combination with gold to capture/transfer released peptides from gold to palladium and/or to lock BSBCA-C6C11 into a more permanent *cis* state.

The above QCM experiments show that *trans*-BSBCA-C6C11 adsorbs on a gold surface faster and with higher affinity than the *cis*-BSBCA-C6C11 peptide (Table 1). In order to interpret the experimental results, we have performed all-atom molecular dynamics simulation (MD) on the peptide–gold systems. MD simulations were performed by starting with peptide configurations located 1.5 nm (mass center to surface) above a (111) gold surface of size $7.105 \, nm \times 7.032 \, nm \times 1.064 \, nm$ in an explicit water box (Figure 3a). In order to identify the binding residues to the gold surface, we have calculated the atom-to-atom pairwise interaction energy between atoms in each residue of a peptide and the gold atoms to show the relative binding strength (Figure S6). For the *trans* configuration the Arg residue stands out as the strongest binder, whereas for the *cis* form there are no distinguishable binding residues signifying that the *cis* confirguration is a weaker binder to gold surface. Previous studies have also demonstrated that the amino acid arginine strongly participates in gold binding.[22, 25] After simulation and equilibration, the results show that the arginine residue and the N-terminus residues of *trans*-BSBCA-C6C11 bind tightly to the gold surface (Figure 3b). Upon isomerization to *cis*-BSBCA-C6C11 in Figure 3c, the arginine residue now faces the water to form a salt bridge with one of the sulfonate groups in the linker leading to a loss of binding affinity with the gold surface. In parallel, we obtained free energy profiles of the adsorption trajectory for *trans*-BSBCA-C6C11 and *cis*-BSBCA-C6C11 on gold (Figure 3d) as a function of potential mean pulling force of peptide away from the surface. Analysis of the two profiles reveal that there is an energy barrier of $\approx 1.5 \, kcal \, mol^{-1}$ at 1.2 nm away from the surface for *cis*-BSBCA-C6C11 and no barrier for *trans*-BSBCA-C6C11. This supports the QCM data that *trans*-BSBCA-C6C11 exhibits faster binding kinetics. Additional differences show that the lowest energy starts at ≈ 0.7 nm for the *cis* configuration but occurs at 0.45 nm for the *trans* form. This implies that *cis*-BSBCA-C6C11 is more flexible within a range between 0.45 nm and 0.7 nm, as demonstrated by the lowest-energy configurations shown in Figures 3b,c. Finally, the adsorption free energies estimated by the difference of being on the surface (0.45 nm and 0.70 nm from the gold surface for the *trans* and the *cis* forms, respectively) and in water (1.8 nm from the gold surface for both) are $-9.05 \, kcal \, mol^{-1}$ and $-8.56 \, kcal \, mol^{-1}$ and agree with the experimental measurements (Table 1). Given the significance of the arginine residue in gold binding, we replaced arginine with a glycine residue to yield a newly synthesized BSBCA-C6C11-R (TSNAVCPTLGCL) peptide. By QCM, the arginine substituted BSBCA-C6C11-R peptide exhibited an order of magnitude lower binding affinity to gold than the non-mutated peptide in both the *trans* and *cis* forms (Table 1).

Studies have shown that differences in peptide affinity can have an appreciable effect on the modification of nanomaterial properties.[6, 26, 27] For example, high-affinity peptides have been shown to constrain the growth of inorganic crystals.[26, 28–31] We exploited the ability to optically control the affinity of peptides towards inorganic surfaces by switching between *trans*-BSBCA-C6C11 and *cis*-BSBCA-C6C11 peptide configurations as an approach to control the synthesis and size properties of gold nanoparticles. Briefly, peptide-coated nanoparticles were synthesized by adding chloroauric acid ($HAuCl_4$), sodium borohydride ($NaBH_4$), and BSBCA-C6C11 peptide in HEPES buffer pH 7.4 in the presence of UV or ambient visible light. Upon exposure to visible light, the stable *trans*-BSBCA-C6C11 peptide produced small gold nanoparticles with average sizes approaching ≈ 0.8 nm by dynamic light scattering (DLS) (1.7 nm by TEM), while the UV-exposed *cis*-BSBCA-C6C11 peptide configuration produced larger gold nanoparticles with sizes of 4.8 nm by DLS and 3.5 nm by TEM (Figure 4, Supplemental Figure S7). In total, these sizes are consistent with their respective binding affinities and other peptide systems.[35] Additionally, BSBCA-C6C11 templated gold nanoparticles exhibited broad plasmon resonance peaks at ≈ 519–532 nm and produced weak blue fluorescence at ≈ 440 nm consistent with similarly sized bio-templated gold nanoparticles (Supplemental Figure S8).[32] The presence of an LSPR peak suggests a mixed size population with some nanoparticles approaching sizes greater than 2 nm. Moreover, we could fine tune nanoparticle sizes by optically switching between *cis*→*trans* or *trans*→*cis* peptide configurations during synthesis. In the *trans*→*cis* case, we used the *trans*-BSBCA-C6C11 peptide to initiate synthesis of gold nanoparticles for 1 h in visible light and then switched the peptide structure to *cis*-BSBCA-C6C11 for an additional hour during synthesis by exposure to UV light. This optical sequence likely produced slow-growing nanoparticles during the first hour due to stronger binding/low dissociation, followed by a rapid growth phase and larger particles obtained during the second hour to yield gold nanoparticle sizes of 2.6 nm. Alternatively, when *cis*-BSBCA-C6C11 was used as the initial template before switching to *trans*-BSBCA-C6C11 with visible light, we obtained gold nanoparticles of equivalent size to using *cis*-BSBCA-C6C11 only for synthesis. This is likely due to the rapid
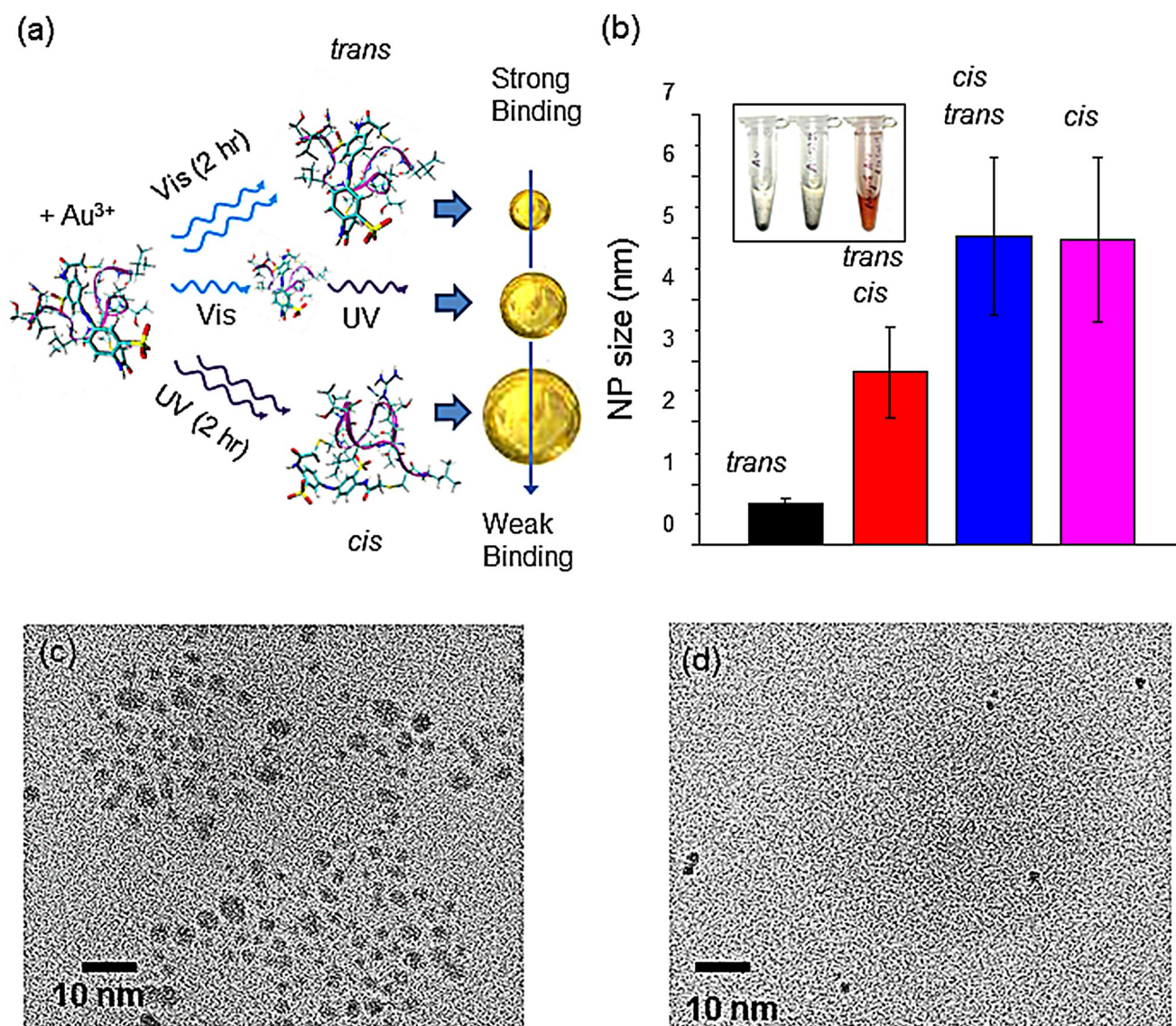
Figure 3. a) Initial setting of molecular modeling systems. b) End-point configuration of *trans*-BSBCA-C6C11 on the gold surface through arginine (R[10]) and the N-terminus. c) End-point configuration of *cis*-BSBCA-C6C11 adsorbed on gold surface through only the N-terminus. d) Free energy profiles during the molecular dynamic simulations of the peptide in *trans* and *cis* conformations pulled away from surface. Reference energy sets to zero when peptides are in water. The x-axis is the distance of the mass-weighted center of the peptides to the gold surface. The y-coordinate is the potential of mean force with the reference energy set to zero when the peptides are in solution (1.8 nm away from surface).

growth of particles followed by a period of strong peptide–gold binding. Peptide binding to gold nanoparticles after synthesis was confirmed by the presence of shifted amide I and amide II bands in the FT-IR spectrum (Figure S9) and visual presence of stable pink and nanoparticle suspensions in water, indicating peptide stabilization (microfuge tubes in Figure 4 b, inset). For the synthesis of gold nanoparticles using the unmodified C6C11 peptide or uncoupled BSBCA cross-linker (no peptide), the sizes were independent of UV or visible light exposure and resulted in gold precipitation in the case of the cross-linker only (Figure 4).

3. Conclusions

The addition of an optical switch to nanoparticle-binding peptides offers a means to control the binding and dissociation of peptides on an inorganic surface, enrich for a single isomer population, and produce a broad spectrum of gold nanoparticle sizes by varying light exposure. By using an intrapeptide cross-linker tethered at 6 and 11 peptide positions, we obtained large changes to the peptide structure in response to photo-isomerization of the cross-linker by UV or visible light exposure. Notably, these structural changes influenced binding affinity due mainly to the arginine residue and formation of a salt bridge favored in the *cis* form. For example, the *trans*-

Figure 4. Photo-tunable synthesis of gold nanoparticles using *trans*-BSBCA-C6C11 and *cis*-BSBCA-C6C11 states. a) Gold nanoparticle synthesis strategy using BSBCA-C6C11 peptide using timed optical pulses to irradiate BSBCA-C6C11 peptide during nanoparticle synthesis. b) DLS size distribution profile of gold nanoparticles synthesized from each optically timed pulse sequence. Inset, left to right: microfuge tubes containing $Au^{3+}/NaBH_4$, $Au^{3+}+BSBCA+NaBH_4$, and $Au^{3+}+BSBCA-C6C11+NaBH_4$. TEM image of gold nanoparticles produced by c) *trans*-BSBCA-C6C11 peptide and d) *cis*-BSBCA-C6C11 peptide, irradiated for 2 h with UV or under visible light.

BSBCA-C6C11 peptide exhibited high gold binding affinities, while the UV exposed *cis*-BSBCA-C6C11 peptide exhibited higher dissociation rates. As a result, we were able to bind and release peptide from a gold surface using light. This process affords a means to recover and reuse peptides released from an inorganic surface with no modifications, enrich for a single isomer using the different binding affinities programmed into peptide, and/or introduce new peptides, polymers, ligands to a partially bare surface to achieve a mixed surface composition. Also, this presents a general approach to replace biomolecular recognition elements from a sensor surface or control the biofunctionalization of surfaces using an optical stimulus. By varying the duration of light exposure and peptide dissociation, we could regulate surface coverage, surface ligand composition, and functionality. These dual binding conformations were also used to tune nanoparticle size as a function of implementing different light pulse cycles. The ability to remotely manipulate peptide structure and its interactions with nanomaterial surfaces via an optical source has huge implications for sensing platforms and would allow sensors to be reconfigured for different targets in the field by simply exchanging biomolecules.

Experimental Section

Synthesis/Conjugation of BSBCA-C6C11 Peptide

C6C11 peptide (TSNAVCPTLRCL) was obtained from Genscript and the BSBCA cross-linker was synthesized separately using a previously reported procedure.[12] For conjugation of the BSBCA cross-linker

to C6C11, 1 mg of lyophilized C6C11 peptide was added at a 1:1 stoichiometry with BSBCA in 2 mL of 0.1 M Tris buffer pH 8.0 in the presence of 3.9 mM TCEP reducing agent under N_2 in a septum sealed 5 mL glass vial. This was incubated at 65 °C in a water bath for 18 hours covered in aluminum foil to prevent light exposure. The BSBCA conjugated peptide was purified on an Amersham Biosciences reversed phase HPLC using a Dupont C_{18} column (9.4 mm×25 cm) to remove unconjugated free peptide at a flow rate of 0.5 mL min^{-1} and linear acetonitrile/water gradient from 2%–100%.

Characterization of Peptide Structure and Light-Induced Isomerization

Circular dichroism spectra were collected on a Jasco J-815 circular dichroism (CD) spectrometer using a 750 μL quartz cuvette and a peptide concentration of 19 μM for both BSBCA-C6C11 and unmodified C6C11 peptides from 180–450 nm with a data pitch of 0.1 nm, bandwidth of 1 nm, scan rate of 50 nm min^{-1}, and averaged over three scans. For photo-isomerization of trans-BSBCA-C6C11 to cis-BSBCA-C6C11, we illuminated the peptide using the fluorescence accessory provided with the CD spectrometer (excitation 365 nm or 450 nm and 500 μm slit width) for 20 minutes and then collected CD spectrum. The actual light intensity of CD illumination measured at 365 nm was 10 mW cm^{-2} and at 450 nm was 9 mW cm^{-2}. CD spectra were also collected as a function of temperature to obtain melting curves. Peptides were heated from 25 °C to 85 °C at 10 °C intervals for 15 minutes using a peltier controlled single cell fluorescence accessory. At each temperature, a CD spectrum was obtained. Melting curves were plotted as a function of ellipticity at 225 nm/201 nm vs. temperature. Theoretical CD spectra were calculated based on their structures obtained from molecular modelling simulations. To measure cis→trans half-lifes of BSBCA cross-linker and BSBCA-C6C11 peptide, we irradiated sample at 365 nm using CD fluorescence accessory for 20 min and immediately measured the absorbance at 365 nm.

Characterization of Binding/Dissociation

A Q-Sense E4 quartz crystal microbalance with dissipation (QCM-D) was used to measure peptide binding. Gold-coated QCM sensors were cleaned via UV–ozone treatment for 10 minutes, followed by heating in a 7.5:1:1 solution of water/30% H_2O_2/NH_4OH at 80 °C for 10 minutes, thorough rinsing with doubly deionized water, and dried with N_2. The clean gold-coated sensors were mounted in a Q-Sense window flow cell module. For peptide binding, we used a peptide concentration of 3.2 μM for all peptides, a flow rate of 0.17 mL min^{-1}, a constant temperature controlled at 23 °C, and monitored the 3rd overtone resonance frequency. For binding of cis-BSBCA-C6C11, we covered the polyethylene flow lines and blocked the sapphire window with aluminum foil to prevent exposure from stray visible light and illuminated the peptide in a 5 mL foil covered glass vial prior to entering the Q-Sense window flow module. Before the flow of peptide was started, we pre-illuminated the peptide for 20 minutes to ensure peptide was in the form of cis-BSBCA-C6C11 before binding. For illumination, we used an Ultrafire 501B UV 365 nm 3W 1-Mode LED Flashlight mounted horizontally ≈5 mm from glass vial or ≈5 mm vertically from sapphire window. The actual light intensity of the UV flashlight was measured to be 25 mW cm^{-2}. To measure in situ peptide dissociation from the gold QCM surface, we irradiated the QCM surface through the sapphire window of QCM module using a vertically mounted Ultrafire 3-W 365 nm LED flashlight fixed at ≈5 mm from surface.

Gold Nanoparticle Synthesis

2.5 μL of 0.1 M $HAuCl_4$ (Sigma) was added with 2.5 μL of 1.9 mM BSBCA-C6C11 peptide or unmodified C6C11 peptide in 500 μL of 0.1 M HEPES buffer pH 7.4 (Amresco). After 5 minutes of incubation of gold salt with peptide, 5 μL of a 0.2 M $NaBH_4$ was added to the gold–peptide solution. The gold–peptide solution was immediately illuminated in a 750 μL quartz cuvette using a circular dichroism spectrometer with fluorescence accessory as the illumination source. For illumination, we used a 500 μm slit width and 365 nm excitation wavelength. TEM images were obtained on a Phillips CM200 transmission electron microscope operating at 200 kV. Samples were prepared by pipetting 10 μL of gold nanoparticles onto a 3 mm 200 mesh copper TEM grid coated with ultrathin carbon film (Ted Pella) and air-dried. Dynamic light scattering (DLS) analysis was obtained on a Malvern Instruments nano series Zetasizer with 500 μL of sample.

Molecular Dynamics Simulations

All structures were constructed using VMD.[33] All molecular dynamics simulations were performed using NAMD.[34] The cis and trans cross-linked peptides were initially located 1.5 nm (mass center to surface) above a (111) gold surface of size 7.105 nm×7.032 nm× 1.064 nm. The recently developed polarizable force field GolP for gold and protein interaction in water was used to model the gold surface. The mixture of GolP and parameters for proteins in CHARMM and NAMD format were kindly provided by Bellucci.[35–38] The parameters for the Azo-liner were taken from Paoli et al.[39] The Azo-linker was initially tilted relative to the gold surface to avoid biasing its interaction with either the gold surface or water. The system was solvated in a TIP3 water box of 6.0 nm height to avoid image interaction. One of the initial configurations is shown in Figure 3 a. Using replica-exchange molecular dynamics simulations, the adsorbed peptide structures were prepared. To calculate the adsorption free energy, we first applied steered molecular dynamics simulations to locate the adsorption trajectory by gradually pulling the peptides away from surface to water with a constant velocity of 0.05 nm ps^{-1} and a spring constant of 10 kcal mol^{-1} Å^{-2}. Then, 1.5 ns equilbration was performed by setting the pulling velocity to zero and constraint force to 3 kcal mol^{-1} Å^{-2} to collect data for each snapshot along the trajectory. The last 0.5 ns data were used to construct the free energy profile using the weighted histogram analysis method (WHAM).[40] A non-bonded cutoff distance of 1.0 nm was used with the application of the switching function starting at 0.9 nm. Periodic boundary conditions were applied in all three dimensions. The particle-mesh Ewald method was used to calculate the long-range electrostatics forces. The recently developed polarizable force field GolP was used in all the simulations. For temperature replica exchange simulations, 64 replicas were used in the temperature range between 280 and 680 K. Exchange attempts were performed every ps. The endpoint configuration at 300.43 K after temperature replica exchange was used for further simulation until the radius of gyration of peptides was converged. For steered molecular dynamics simulations, a constant velocity of 0.05 nm ps^{-1} and a spring constant of 10 kcal mol^{-1} Å^{-2} was used to pull the peptide with the cross-linker together.

[1] K. E. Sapsford, W. R. Algar, L. Berti, K. B. Gemmill, B. J. Casey, E. Oh, M. H. Stewart, I. L. Medintz, *Chem. Rev.* **2013**, *113*, 1904.

[2] M. B. Dickerson, K. H. Sandhage, R. R. Naik, *Chem. Rev.* **2008**, *108*, 4935.

[3] W. J. Crookes-Goodson, J. M. Slocik, R. R. Naik, *Chem. Soc. Rev.* **2008**, *37*, 2403.

[4] J. C. Y. Kah, E. L. L. Yeo, W. L. Koh, B. E. A. Poinard, D. J. H. Neo, *Crit. Rev. Biomed. Eng.* **2013**, *41*, 323.

[5] A. A. Shemetov, I. Nabiev, A. Sukhanova, *ACS Nano* **2012**, *6*, 4585.

[6] R. Coppage, J. M. Slocik, H. Ramezani-Dakhel, N. M. Bedford, H. Heinz, R. R. Naik, M. R. Knecht, *J. Am. Chem. Soc.* **2013**, *135*, 11048.

[7] J. Luo, M. M. Maye, L. Han, N. N. Kariuki, V. W. Jones, Y. Lin, M. H. Engelhard, C.-J. Zhong, *Langmuir* **2004**, *20*, 4254.

[8] S. I. Stoeva, V. Zaikovski, B. L. V. Prasad, P. K. Stoimenov, C. M. Sorensen, K. J. Klabunde, *Langmuir* **2005**, *21*, 10280.

[9] W. Szymański, J. M. Beierle, H. A. V. Kistemaker, W. A. Velema, B. L. Feringa, *Chem. Rev.* **2013**, *113*, 6114.

[10] S. Dinçer, C. Tamerler, M. Sarikaya, E. Pişkin, *Surf. Sci.* **2008**, *602*, 1757.

[11] A. Nomura, A. Okamoto, *Chem. Commun.* **2008**, 1906 – 1908.

[12] D. C. Burns, Z. Fuzhong, G. A. Woolley, *Nat. Protoc.* **2007**, *2*, 251.

[13] A. A. Beharry, G. A. Woolley, *Chem. Soc. Rev.* **2011**, *40*, 4422.

[14] Z. Tang, J. P. Palafox-Hernandez, W.-C. Law, Z. E. Hughes, M. T. Swihart, P. N. Prasad, M. R. Knecht, T. R. Walsh, *ACS Nano* **2013**, *7*, 9632.

[15] A. J. Rowe, *Methods* **2011**, *54*, 157.

[16] A. N. Volkov, *Acc. Chem. Res.* **2015**, *48*, 3036.

[17] J. P. Palafox-Hernandez, C.-K. Lim, Z. Tang, K. L. M. Drew, Z. E. Hughes, Y. Li, M. T. Swihart, P. N. Prasad, M. R. Knecht, T. R. Walsh, *ACS Appl. Mater. Interfaces* **2016**, *8*, 1050.

[18] Z. H. Zhang, D. C. Burns, J. R. Kumita, O. S. Smart, G. A. Woolley, *Bioconjugate Chem.* **2003**, *14*, 824.

[19] A. L. Rucker, T. P. Creamer, *Protein Sci.* **2002**, *11*, 980.

[20] A. A. Adzhubei, M. J. E. Sternberg, A. A. Makarov, *J. Mol. Biol.* **2013**, *425*, 2100.

[21] S. Samanta, G. A. Woolley, *ChemBioChem* **2011**, *12*, 1712.

[22] J. M. Slocik, R. R. Naik, *Chem. Soc. Rev.* **2010**, *39*, 3454.

[23] M. Hnilova, E. E. Oren, U. O. S. Seker, B. R. Wilson, S. Collino, J. S. Evans, C. Tamerler, M. Sarikaya, *Langmuir* **2008**, *24*, 12440.

[24] G. Blanco-Brieva, M. Pilar de Frutos Escrig, J. M. Campos-Martin, J. L. G. Fierro, *Green Chem.* **2010**, *12*, 1163.

[25] L. B. Wright, P. M. Rodger, S. Corni, T. R. Walsh, *J. Chem. Theory Comput.* **2013**, *9*, 1616.

[26] R. Coppage, J. M. Slocik, B. D. Briggs, A. I. Frenkel, R. R. Naik, M. R. Knecht, *ACS Nano* **2012**, *6*, 1625.

[27] S. N. Kim, Z. F. Kuang, J. M. Slocik, S. E. Jones, Y. Cui, B. L. Farmer, M. C. McAlpine, R. R. Naik, *J. Am. Chem. Soc.* **2011**, *133*, 14480.

[28] C. Y. Chiu, Y. J. Li, L. Y. Ruan, X. C. Ye, C. B. Murray, Y. Huang, *Nat. Chem.* **2011**, *3*, 393.

[29] Y. Li, Y. Huang, *Adv. Mater.* **2010**, *22*, 1.

[30] L. Ruan, C.-Y. Chiu, Y. Li, Y. Huang, *Nano Lett.* **2011**, *11*, 3040.

[31] J. P. Palafox-Hernandez, Z. Tang, Z. E. Hughes, Y. Li, M. T. Swihart, P. N. Prasad, T. R. Walsh, M. R. Knecht, *Chem. Mater.* **2014**, *26*, 4960.

[32] B. Sharma, D. D. Purkayastha, S. Hazra, M. Thajamanbi, C. R. Bhattacharjee, N. N. Ghosh, J. Rout, *Bioprocess Biosyst. Eng.* **2014**, *37*, 2559.

[33] W. Humphrey, A. Dalke, K. Schulten, *J. Molec. Graphics* **1996**, *14*, 33.

[34] J. C. Phillips, R. Brgoldn, W. Wang, J. Gumbart, E. Tajkhorshid, E. Villa, C. Chipot, R. D. Skeel, L. Kale, K. Schulten, *J. Comput. Chem.* **2005**, *26*, 1781.

[35] L. Bellucci, S. Corni, *J. Phys. Chem. C* **2014**, *118*, 11357.

[36] F. Lori, S. Corni, *J. Comput. Chem.* **2008**, *29*, 1656.

[37] F. Lori, R. Di Felice, E. Molinari, S. Corni, *J. Comput. Chem.* **2009**, *30*, 1465.

[38] L. Bellucci, G. Brancolini, A. Calzolari, O. C. Parramon, S. Corni, R. Di Felice, *ACS Symp. Ser.* **2012**, *1120*, 229.

[39] B. Paoli, M. Seeber, E. H. Backus, J. A. Ihalainen, P. Hamm, A. Caflisch, *J. Phys. Chem. B* **2009**, *113*, 4435.

[40] A. Grossfield, *WHAM: the weighted histogram analysis method*, Version 2.0.9, **2013**, http://membrane.urmc.rochester.edu/content/wham.